



# Chemo–mechanical modeling for prediction of alkali silica reaction (ASR) expansion

Stéphane Multon<sup>\*</sup>, Alain Sellier, Martin Cyr

Université de Toulouse, UPS, INSA, LMDC (Laboratoire Matériaux et Durabilité des Constructions), 135, avenue de Rangueil, F-31 077 Toulouse Cedex 04, France

## ARTICLE INFO

### Article history:

Received 1 July 2008

Accepted 11 March 2009

### Keywords:

Alkali–silica reaction (ASR)

Particle size

Alkali content

Expansion

Model

## ABSTRACT

The effect of the size of the aggregate on ASR expansion has already been well illustrated. This paper presents a microscopic model to analyze the development of ASR expansion of mortars containing reactive aggregate of different sizes. The attack of the reactive silica by alkali was determined through the mass balance equation, which controls the diffusion mechanism in the aggregate and the fixation of the alkali in the ASR gels. The mechanical part of the model is based on the damage theory in order to assess the decrease of stiffness of the mortar due to cracking caused by ASR and to calculate the expansion of a Representative Elementary Volume (REV) of concrete. Parameters of the model were estimated by curve fitting the expansions of four experimental mortars. The paper shows that the decrease of expansion with the size of the aggregate and the increase of the expansion with the alkali content are reproduced by the model, which is able to predict the expansions of six other mortars containing two sizes of reactive aggregate and cast with two alkali contents.

© 2009 Elsevier Ltd. All rights reserved.

## 1. Introduction

Alkali Silica Reaction is a chemical reaction between the alkalis of cement and the reactive silica of concrete structure aggregates. The reaction products are expansive gels which induce stresses, and hence cracking, in concrete. The main research on ASR concerns the expert appraisal of damaged structures [1–5]. Modeling ASR and the resulting expansion are necessary to obtain relevant predictions of the structural responses of damaged structures and models must take the chemical and physical aspects into account.

The LMDC (Laboratoire des Matériaux et Durabilité des Constructions), with EDF (Electricité de France) as a partner, has been working to establish a general method for the reassessment of ASR-damaged structures. The method uses expansion measurements on small specimens ( $2 \times 2 \times 16$  cm) of mortar cast with crushed aggregates extracted from damaged structures [6,7] in order to evaluate the advancement of the reaction on the aggregates. As shown in [6,7], the advancement varies with the size of the aggregates because of the time taken for alkali to diffuse into the aggregate. One of the advantages of this method is that it performs calculations by using the state of advancement of the different aggregate sizes in the structure concrete, which allows relevant predictions to be obtained. However, this research needs to be completed by the development of microscopic modeling that uses the tests proposed in [6,7] in a reliable way, particularly according to the effect of the alkali content and the size of the reactive aggregate particles on the ASR-expansions. Predicting the expansion of concrete in real dama-

ged structures is the final aim of this model. However, as a first step, it is used here to analyze laboratory experiments where the effects of mechanical stresses and environmental conditions on expansion are not considered. Similarly, alkali regeneration by calcium ions, which is a slow process [8–10], is not taken into account.

This paper deals with the development of an empirical microscopic ASR model. The main input data to such models are alkali and reactive silica contents, aggregate sizes, and mechanical properties of the mortar. The main result is the prediction of the ASR expansion of the concrete taking into consideration the physicochemical mechanisms of the reaction. Among the existing microscopic ASR models, some were developed to take the mechanics of ASR into consideration [11,12], and others focus on the chemical phenomena [13]. Finally, some models take both aspects into account [14–18]. Many phenomena of ASR can be described by the existing models (e.g. diffusion of alkali into the aggregates, gel permeation and imbibition); but others cannot be correctly represented yet (e.g. evolution of the concentration of alkali during the reaction, and expansion of concrete containing different sizes of reactive aggregate).

The microscopic model developed in this paper is based on some of these previous models [13,14,17,18]. It can predict the damage and the expansion of a Representative Elementary Volume (REV) of concrete containing a mix of reactive aggregates of different sizes. The diffusion of alkali into the aggregate is taken into account; the production of the ASR gel increases with the molar concentration of alkalis in the aggregate. In the cement paste surrounding the reactive aggregate, the concentration of alkalis decreases with their diffusion towards the aggregate and their consumption by the ASR gel. The gel permeates into a part of the porous volume connected to the reactive aggregate. Once the available porous volume has been

<sup>\*</sup> Corresponding author.

E-mail address: [multon@insa-toulouse.fr](mailto:multon@insa-toulouse.fr) (S. Multon).

filled by the gel, the pressure due to ASR acts on the surrounding cement paste, leading to damage and expansion.

The modeling principles and assumptions are first presented and discussed. Then, the physicochemical and mechanical models are developed in two parts. Finally, the model is used to calculate the expansion of ten mortars containing different amounts of two sizes of reactive aggregate and having two alkali contents. Five parameters of the physicochemical model cannot be obtained by direct measurements and are therefore calculated by inverse analysis using four of the ten mortars. The parameters thus obtained are used to predict the expansions of the other six mortars. Once the mechanical characteristics of the sound concrete are known, no additional fitting of parameters is necessary for the mechanical modeling. The last part points out the qualities and the limitations of the model and gives some indications as to how it could be improved.

## 2. Principles

### 2.1. Physicochemistry and mechanics of ASR

As in previous works [13,15,18], the model developed in this paper used the reaction mechanisms presented by Dent Glasser and Kataoka [19]:

- The first part of the reaction is the diffusion of the alkali and hydroxyl ions into the reactive aggregate, and the destruction of the silanol and siloxane bonds contained in the reactive silica.
- The second part is the formation of the ASR gels in the presence of water and calcium ions [19–21]. Once formed, the gel permeates through a part of the connected porous volume between aggregate and cement paste and fills a part of the connected porosity [22]. Then the gel exerts a pressure on the cement paste, which causes cracking and expansion of the concrete.

Moreover, in order to complete the physical considerations, assumptions based on numerous experimentations already published were made: the existence of a threshold in alkali concentration under which ASR does not occur [23–26], the high nonlinearity of the dissolution of the reactive silica with pH [29] and the stoichiometry of ASR gels [30–32].

### 2.2. Assumptions

It is not possible to consider all the physical and chemical mechanisms of such a reaction occurring in a complex medium like concrete. Simplifications have to be assumed in order to model ASR expansion in accordance with most phenomena.

#### 2.2.1. Geometry

The reactive aggregate and the Relative Elementary Volume (REV) of concrete surrounding the reactive aggregate are assumed to be

spherical (Fig. 1). The radius of the REV depends on the radius and the content of the reactive aggregate in concrete, as given by Eq. (1) [18]:

$$R_{\text{REV}}^a = \frac{R_a}{\sqrt[3]{\phi_a \cdot C_{\text{agg}}}} \quad (1)$$

with:

- $a$ , a superscript relative to the size fraction of the reactive aggregate with mean radius  $R_a$
- $R_{\text{REV}}^a$  the REV radius corresponding to the aggregate size fraction  $a$
- $\phi_a$  the volume fraction of reactive aggregates with mean radius  $R_a$
- $C_{\text{agg}}$  the volume fraction of all the aggregate per  $\text{m}^3$  of concrete.

The number of reactive aggregates per  $\text{m}^3$  of concrete  $N_a$  is equal to:

$$N_a = \frac{\phi_a \cdot C_{\text{agg}}}{\frac{4}{3}\pi R_a^3} \quad (2)$$

#### 2.2.2. Diffusion of alkali and attack of reactive silica

In the model presented in [18], the diffusion of the ionic species into both reactive aggregate and cement paste surrounding the aggregate is considered. However, at each time step, the concentrations of ionic species are roughly homogeneous in the cement paste. This can be explained by the differences between the coefficients of diffusion in the cement paste (about  $10^{-11} \text{ m}^2/\text{s}$ ) and in the aggregate (about  $10^{-15} \text{ m}^2/\text{s}$ ). Thus, diffusion into the cement paste appears to be instantaneous compared to diffusion into the aggregate, so the alkali concentration was assumed to be uniform in the paste in the present model. This constitutes the main simplification in relation to Poyet's modeling [18].

Moreover, the aggregate was taken as spherical. Thus the concentrations of the ionic species diffusing into the aggregate depend only on the time and on the radius  $r$  from the centre of the reactive aggregate (Fig. 2).

Several authors showed that no expansion occurred in concrete containing alkali silica reactive aggregate for low alkali contents: under a threshold lying between 3 and 5  $\text{kg}/\text{m}^3$  [23–26] or for an alkali concentration lower than 0.5 or 0.6  $\text{mol}/\text{l}$  of  $\text{Na}^+$  [27,28]. Urhan reports that the solubility of silica is quite constant in a solution having a pH of less than 9 or 10 but increases rapidly for higher pH [29]. Due to the high nonlinearity between the pH and the solubility of the silica and to the relationship between the value of the pH in a solution and the concentration of alkali, the destruction of the reactive silica was assumed to increase significantly when the concentration of alkalis in a part of the aggregate was higher than a threshold concentration noted  $Na_{\text{th}}$ . When the threshold is reached

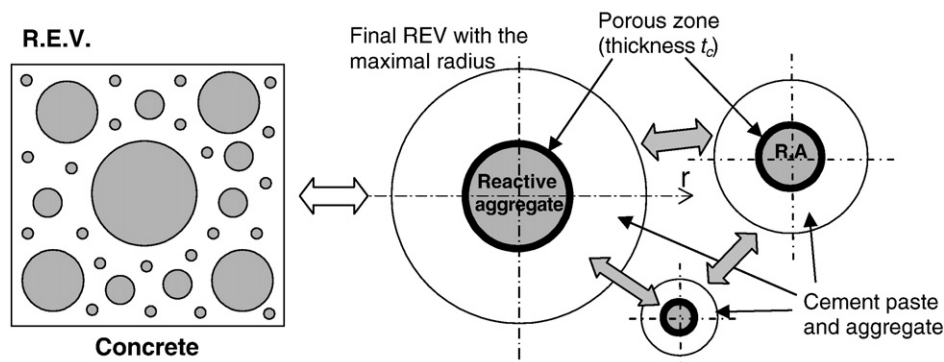


Fig. 1. Definition of the Relative Elementary Volume for several reactive aggregate sizes [18].

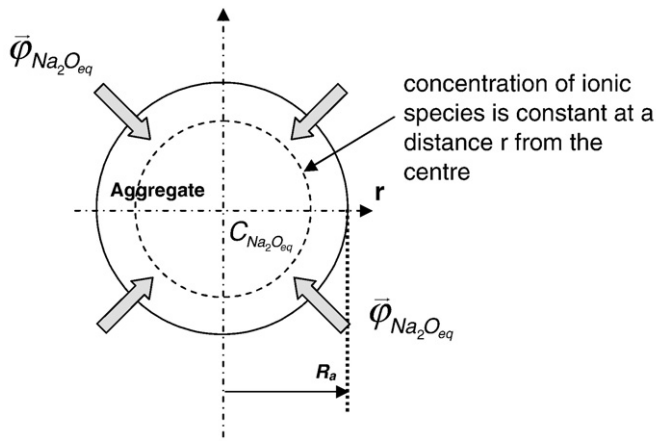


Fig. 2. Diffusion of  $\text{Na}_2\text{O}_{\text{eq}}$  in aggregate.

and passed, the present model assumes that gel formation increases with a rate proportional to the difference between the alkali concentration in the aggregate and the threshold. The same rate is taken for the alkali consumption by the ASR gels. Therefore, the kinetics of the reaction, and thus of the gel formation, is assumed to be controlled by the destruction of the reactive silica due to alkali diffusion. Some authors [8–10] consider that the gel formation depends on the presence of calcium ions. This has not been taken into account in the model. However, as calcium is provided by portlandite dissolution and as this dissolution is not possible while the alkali content is high, the need for calcium can be neglected during the first step of an accelerated test. This aspect of the reaction will have to be carefully considered for the simulation of long-term ASR phenomena. So the extension of the present model to structural applications will have to include calcium substitution.

### 2.2.3. ASR gel

Another problem for ASR modeling concerns the assumptions on the compositions of the gels produced by the reaction. The compositions of the gels depend on many parameters, such as gel position in the concrete (in or out of the aggregate) and its age (it is usually assumed that old gels contain more calcium than new). The  $\text{Na}_2\text{O}/\text{SiO}_2$  ratio in the gels varies from about 0.1 to 0.4 [30–32]. It is quite difficult to obtain a relevant and representative value for the gel composition. In the model presented here, the  $\text{Na}_2\text{O}/\text{SiO}_2$  ratio is assumed to be equal to the mean value 0.2 obtained in laboratory experiments in [32]; it is assumed that 1 mol of  $\text{Na}_2\text{O}_{\text{eq}}$  reacts with 5 mol of  $\text{SiO}_2$  to give 1 mol of ASR gel. The volume of gel produced by one size of aggregate  $n_g^a$  is obtained by multiplying the number of moles of ASR gel produced by the aggregate  $a$  by the molar volume of the gel  $V_{\text{gel}}^{\text{mol}}$  (in  $\text{m}^3/\text{mol}$ ). The total volume of gel formed is then the sum of the volume of gel produced by all the aggregates (in  $\text{m}^3$ ):

$$V_g = \sum_i n_g^a \times V_{\text{gel}}^{\text{mol}} \quad (3)$$

As described just above, after its formation, the gel can permeate through a part of the connected porous volume surrounding the aggregate [33] or can stay in the cracks of the aggregate. This part of connected porosity is modeled as a volume of porosity totally filled by the gel with an equivalent thickness  $t_c$  (Fig. 1, Eq. (4)). The equivalent thickness is assumed not to change with the size of the aggregate. Thus, the volume of gel necessary to fill this porosity,

which consequently which does not exert pressure, is equal to the connected porosity ( $p$ ):

$$V_{\text{por}} = \frac{4}{3}\pi((R_a + t_c)^3 - R_a^3) \cdot p \quad (4)$$

The larger the aggregate size, the lower the ratio 'connected porous volume/aggregate volume'. Therefore the largest aggregate causes the largest ASR-expansion.

### 2.2.4. Mechanical considerations

The model is supposed to calculate ASR expansion for stress free specimens. Moreover, the mechanical properties are taken to be isotropic and, thus, the mechanical behavior of the aggregate and of the cement paste in the REV is taken as isotropic. The behaviors of the two media are assumed to be elastic for stresses lower than their compressive and tensile strengths. The expansions due to ASR occur over long periods. During the process, the materials are not subjected to instantaneous loading but to progressive stresses which cause creep strains in the concrete [5]. In order to take the effect of concrete creep on the ASR expansion into account, the calculations are performed with a long-term Young's modulus equal to a third of the instantaneous Young's modulus (which is the usual value used in the French reinforced concrete design code [34]). For the same stress, using the long-term modulus rather than the instantaneous modulus leads to larger strains. The strains are then equal to the sum of the instantaneous strains due to the ASR gel pressure and the creep strains of the cement paste under the ASR gel pressure. If the stresses become higher than the tensile strengths of the materials, cracking and damage occur in the concrete. In the following calculations, the crack density is consistent with the damage to the concrete calculated by the model (the damage is defined as the decrease of the long-term Young's modulus due to cracking). After cracking, the gel is assumed to permeate into the cracks.

## 3. Physicochemical modeling

The physicochemical modeling concerns the diffusion of the alkali ions into the aggregate and the formation of the ASR gel. The alkali diffusion into the aggregate is controlled by the mass balance equation with a depletion term to represent the consumption of alkali during the formation of the ASR gel. The volume of gel produced by the reaction can then be calculated from the alkali consumed in the mass balance equation. The equations are solved numerically by using a geometrical discretization based on finite volumes and time discretization by Euler's method.

### 3.1. Mass balance equation

#### 3.1.1. Alkali diffusion in aggregate

Just after casting, the alkali concentration is high in the cement paste and negligible in the aggregate. Therefore, a flux of alkali ( $\text{Na}^+$  and  $\text{K}^+$ ) appears between the cement paste and the core of the aggregate. The mass balance of alkali in the aggregate with the assumed spherical symmetry can be described by the equation:

$$\frac{\partial}{\partial t}(p_{\text{agg}} S_r C_{\text{Na}}) = \frac{1}{r^2} \frac{\partial}{\partial r} \left( D \cdot r^2 \frac{dC_{\text{Na}}}{dr} \right) + S(C_{\text{Na}}) \quad (5)$$

with:

$t$	the time
$p_{\text{agg}}$	the porosity of the aggregate,
$S_r$	the saturation degree,
$C_{\text{Na}}$	the concentration of alkali ( $\text{Na}^+$ and $\text{K}^+$ ),
$r$	the distance from the center of the aggregate,
$D$	coefficient of diffusion of alkalis into the aggregate,
and $S(C_{\text{Na}})$	the depletion term that represents alkali consumption.

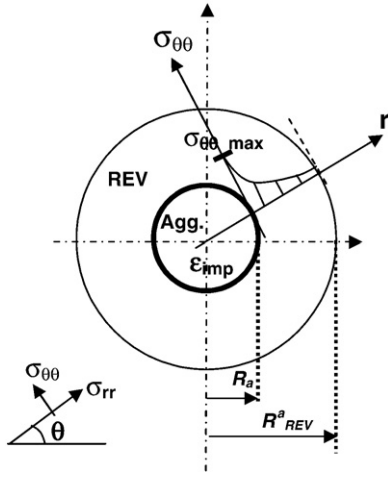


Fig. 3. Tensile stress in the REV subjected to ASR induced strains.

In order to solve the equation, two boundary conditions were used:

- at the centre of the aggregate ( $r=0$ ), the flux is equal to zero;
- at the external boundary ( $r=R_a$ ), the alkali concentration is equal to  $C_{Na}^p$ , the alkali concentration in the cement paste. For the initial condition, this concentration is equal to:

$$C_{Na}^{cp} = 2 \times \frac{M_{Na2O}}{M_{Na2O}^{mol}} \times \frac{1}{p_{cp} S_r (1 - C_{agg})} \quad (6)$$

with

$$p_{cp} = \frac{p_{mort} - p_{agg} \cdot C_{agg}}{(1 - C_{agg})} \quad (7)$$

with:

$M_{Na2O}$  the mass of equivalent alkali per  $m^3$  of concrete,  
 $M_{Na2O}^{mol}$  the molar mass of equivalent alkali (equal to 0.062 kg/mol),  
 $p_{cp}$ ,  $p_{mort}$ ,  $p_{agg}$  the porosity of the cement paste, mortar, and aggregate respectively,  
 and  $C_{agg}$  the aggregate concentration per  $m^3$  of concrete.

During the process, the concentration of alkali in the cement paste decreases due to alkali diffusion into the aggregate (see next part).

### 3.1.2. Alkali concentration in the cement paste

The variation of alkali content in the cement paste is due to the diffusion from the paste to the aggregate. It is equal to the sum of the flux of alkali at the boundary ( $r=R_a$ ) between all the aggregate and the paste. For concrete containing several size fractions,  $a$ , of reactive aggregate, the flux has to be summed over all of them. It can be calculated by:

$$\frac{\partial}{\partial t} (p_{cp} S_r C_{Na}) = \sum_a N_a \cdot D \cdot 4\pi R_a^2 \frac{dC_{Na}^a}{dr} (R_a) \quad (8)$$

with  $N_a$  the number of reactive aggregates (Eq. (2)).

### 3.1.3. Consumption of alkalis

As explained in the 'Assumptions' section, the consumption kinetics of alkalis is assumed to be proportional to the difference

between the concentration of alkali in the aggregate and the threshold above which the silica dissolution starts. Thus, the depletion term of the mass balance equation is:

$$S(C_{Na}) = f(C_{Na} - Na_{thr})^+ \quad (9)$$

with  $f$ , the alkali fixation coefficient. This is the coefficient of proportionality between the consumption kinetics of alkali and the difference between the concentration of alkali in the aggregate and the alkali threshold.  $f$  is a negative parameter. Note that it could depend on the temperature if AAR dependence on temperature is to be modeled.

$(X)^+$  is equal to  $X$  if  $X > 0$  or equal to 0 if  $X \leq 0$ .

$S(C_{Na2O})$  is the amount of alkali fixed per  $m^3$  of aggregate. If the concentration of alkalis in the aggregate is lower than the alkali threshold, the term is zero; there is no consumption of alkali and no ASR-gel formation. If the concentration is higher than the threshold, the consumption of alkali starts with the kinetics given by Eq. (9).

Moreover, the consumption of alkali has to be stopped when all the reactive silica contained in the aggregate has reacted with alkali. As the  $Na_2O/SiO_2$  ratio of the gel is assumed to be equal to 0.2 [32], the end of the alkali fixation is obtained when the amount of alkali fixed by the aggregate is equal to 0.2 times the reactive silica content of the aggregate.

Note: The unit of the alkali fixation coefficient is (mol/ $m^3$  of aggregate) per (mol/ $m^3$  of solution) per second.

### 3.2. Formation of the ASR gel

The number of moles of ASR gel produced in the aggregate  $a$  at time step  $t$  is equal to the number of moles of  $Na_2O$  consumed by the reaction, thus half the number of moles of  $Na^+$ :

$$n_g^a = \frac{4}{3} \pi R_a^3 \times \int_0^t \frac{S(C_{Na})}{2} dt \quad (10)$$

Finally, the volume of gel produced by the reaction is given by the Eq. (3).

## 4. Mechanical modeling

The main result of the chemical modeling is  $V_g$ , the volume of ASR gel formed by the reaction. The volume of gel is then used to determine the strain induced on the REV and finally the expansion of the damaged concrete caused by the chemical reaction. As for the chemical modeling, the equations of mechanical equilibrium are calculated on the spherical REV, as has already been described for elastic conditions in [11,14,17]. In the REV, the mechanical equations are used for two media:  $a$ , the aggregate under study, and SC, the concrete surrounding the studied aggregate (medium including cement paste and other aggregate – Fig. 3). The cracking due to ASR is taken into account by isotropic mechanical damage [35,36]. Thus, the mechanical problem is assumed to be non-linear elastic due to the introduction of the damage variable. The equations developed below present an analytical solution and are applied to each aggregate size.

### 4.1. Strain–stress equations

The ASR gel is supposed to be incompressible compared to the elastic properties of the cement paste and aggregate. Therefore, the ASR expansion can be taken into account as an imposed strain in the aggregate elastic constitutive law:

$$\underline{\underline{\sigma_a}} = \lambda_a tr \underline{\underline{\varepsilon_a}} \cdot \underline{\underline{I}} + 2 \cdot \mu_a \cdot \underline{\underline{\varepsilon_a}} - (3\lambda_a + 2\mu_a) \cdot \underline{\underline{\varepsilon_{imp1}}}(t) \quad (11)$$



The constitutive law of the medium SC only considers the elastic effect of the material:

$$\underline{\underline{\sigma}}_{SC} = \lambda_{SC} \text{tr} \underline{\underline{\varepsilon}}_{SC} \cdot \underline{\underline{I}} + 2 \cdot \mu_{SC} \cdot \underline{\underline{\varepsilon}}_{SC} \quad (12)$$

with

$\underline{\underline{\sigma}}$  the stress matrix for each material,  
 $\underline{\underline{\varepsilon}}$  the strain matrix for each material,  
 $\underline{\underline{I}}$  the unit matrix,

$\lambda$  and  $\mu$  are, for each material:

$$\lambda = \frac{E\nu}{(1+\nu)(1-2\nu)} \quad (13)$$

and

$$\mu = \frac{E}{2 \cdot (1+\nu)} \quad (14)$$

where  $E$  is the Young's modulus and  $\nu$ , the Poisson's coefficient of the medium.  $\varepsilon_{\text{imp1}}$  is the imposed strain applied to the aggregate.

The imposed strain applied to the aggregate is isotropic. It is assessed from the increase in volume due to gel formation; the details of the calculation are given below (Eq. (23)).

The displacements in the materials are deduced by solving the equilibrium equation of the elastic solids  $\text{div} \underline{\underline{\sigma}} = 0$  assuming spherical symmetry. Displacements  $u_a$  in the aggregate and  $u_{SC}$  in the surrounding concrete then depend only on the radius  $r$ :

$$\text{In the aggregate } a: \quad u_a(r) = A_a \cdot r \cdot \underline{\underline{e}}_r \quad (15)$$

$$\text{In the surrounding concrete SC:} \quad u_{SC}(r) = \left( A_{SC} \cdot r + \frac{B_{SC}}{r^2} \right) \cdot \underline{\underline{e}}_r \quad (16)$$

The three unknown constants ( $A_a$ ,  $A_{SC}$  and  $B_{SC}$ ) are determined from the following boundary conditions (Fig. 3):

- The radial displacements at the boundary between the aggregate and the surrounding concrete are equal;
- The radial stresses are continuous at the boundary between the aggregate and the surrounding concrete;
- The radial stress on the external surface is equal to zero (unloaded REV) (note: this assumption leads to a free swelling model).

The mechanical equations can thus be solved and the variation of the stresses in the two media can be analyzed. Due to the gel swelling, the aggregate is subjected to an isotropic stress (pressure). This pressure is balanced by radial compressive stress in the concrete surrounding the aggregate (decreasing from the aggregate pressure (at  $R_a$ ) to zero on the REV external surface), and tensile stress in the tangential directions. The variation of the tensile stress in the tangential directions  $\sigma_{\theta\theta}$  and  $\sigma_{\varphi\varphi}$  with the radius has been plotted in Fig. 3. The maximum tensile stress is located at the boundary between the aggregate and the surrounding concrete. As the strength of concrete is higher in compression ( $f_c$ ) than in tension ( $f_t$ ), radial cracks due to the tensile stresses appear first and damage the surrounding concrete zone between the aggregate ( $R_a$ ) and a radius  $R_d$  ( $R_d - R_a$  corresponds to the crack length). In the following section, the damage theory is used to replace the cracked concrete by an equivalent concrete with a reduced Young's modulus. This modeling has the advantage of leading to an equivalent elastic problem, governed by the same set of equations as the previous ones, but with a lower Young's modulus.

#### 4.2. Damaged REV

##### 4.2.1. Damaged Young's modulus of the REV

The REV contains several reactive aggregates (Fig. 1), which all cause cracks in the REV. The interactions between the cracks of the different aggregates in the REV cause a decrease in the concrete modulus. This can be modeled by a damage variable [35]. The damage evaluation method is based on the strain equivalence principle [36]: the cracked medium (initial Young's modulus  $E_0$ ) is replaced by an equivalent medium without cracks but with a lower modulus  $E_d$  (Fig. 4) leading to the same displacement as the cracked one with the initial Young's modulus. Therefore, as the cracked zone cannot withstand radial tension exceeding the tensile strength, the residual uncracked surrounding concrete is equivalent to a hollow sphere with inner and outer radii equal to  $R_d$  and  $R_{\text{REV}}$  under pressure  $p$ . According to the strain equivalence principle, the radial strain of this hollow sphere must be equal to the radial strain of the uncracked hollow sphere with inner and outer radii equal to  $R_a$  and  $R_{\text{REV}}$  under pressure  $p$  but with a damaged Young modulus  $E_d$  (Fig. 4). The damaged variable is then defined by:

$$d = 1 - \frac{E_d}{E_0} \quad (17)$$

Thus, the first hollow sphere, with a modulus of  $E_0$ , and the second one, with a modulus of  $(1-d)E_0$  (Fig. 4), have the same stiffness. If the

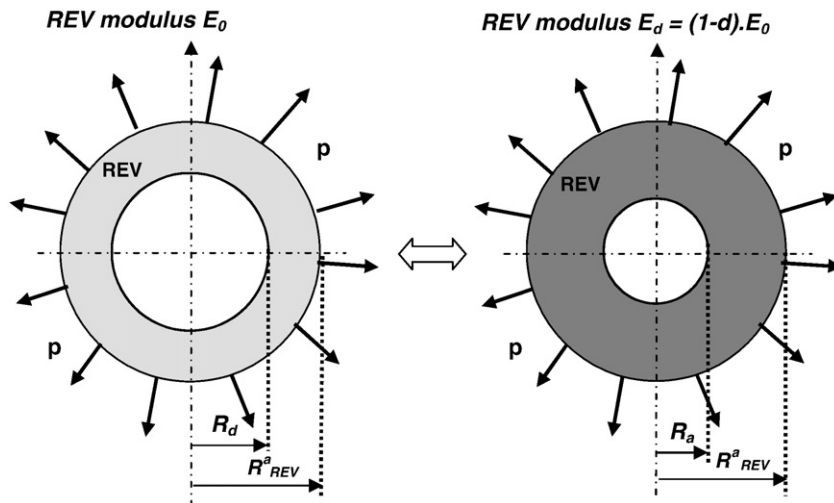


Fig. 4. Determination of the modulus of the damaged concrete.

inner radius  $R_d$  of the first sphere is equal to  $R_a$ , the strain of the cracked medium is equal to the strain of the medium without cracks and the damage  $d$  is equal to 0. If the inner radius  $R_d$  of the first sphere becomes close to the outer radius  $R_{REV}^a$ , the strain of the cracked medium increases and the damage  $d$  increases towards 1. Calculations are successively performed for all the aggregate size fractions  $a$ , and the maximum value of damage is used to determine the modulus of the equivalent medium  $E_d$ :

$$E_d = (1 - d)E_0 \quad (18)$$

#### 4.2.2. Evaluation of the REV expansion

Finally, the mechanical problem studied to assess the ASR expansion is presented in Fig. 5. As explained above, the model assumes that the cracks close to the aggregate are filled by the ASR gels. Thus, three parts can be distinguished (Fig. 5): the central aggregate (between radii 0 and  $R_a$ ), the cracked zone filled by the gel (between radii  $R_a$  and  $R_{cz}$ ) and the part of the REV not yet cracked. As the gel reaches the cracks connected to the reactive aggregate, the radius  $R_{cz}$  corresponds to the radius  $R_d$  used to determine the damage (Fig. 4). The gel pressure is constant in both the aggregate and the cracked zone; it is then applied to the internal boundary of the surrounding uncracked concrete. The modulus of the whole medium surrounding the aggregate is equal to  $E_d$  according to the damaged Young's modulus evaluated just above. The following behavior equation, concerning the part of the REV surrounding the aggregate and filled by the ASR gel, had to be added:

- the constitutive law:

$$\sigma_{cz} = \lambda_{fg} tr \varepsilon_{cz} \cdot I + 2 \cdot \mu_{cz} \cdot \varepsilon_{cz} - (3\lambda_{cz} + 2\mu_{cz}) \cdot \varepsilon_{imp2}(t) \quad (19)$$

where

$\varepsilon_{imp2}$  is the imposed strain applied to the cracked zone of the surrounding concrete due to presence of ASR gel in the cracks;

the displacement is

$$u_{cz}(r) = \left( A_{cz} \cdot r + \frac{B_{cz}}{r^2} \right) \cdot e_r \quad (20)$$

The two supplementary unknown constants  $A_{cz}$  and  $B_{cz}$  can be determined from two supplementary boundary conditions: the continuity of radial displacements and radial stresses at the boundary

between the cracked zone and the surrounding concrete. The mechanical equations can thus be solved in function of  $R_{cz}$ ,  $\varepsilon_{imp1}$  and  $\varepsilon_{imp2}$ . Three last equations are needed to assess the three unknown values of  $R_{cz}$ ,  $\varepsilon_{imp1}$  and  $\varepsilon_{imp2}$ . The tensile stress  $\sigma_{\theta\theta}$  is equal to the concrete tensile strength  $f_t$  for the radius  $R_{cz}$ :

$$\sigma_{\theta\theta}^{SC}(R_{cz}) = f_t \quad (21)$$

The effect of the imposed deformations  $\varepsilon_{imp1}$  and  $\varepsilon_{imp2}$  in the aggregate and in the concrete filled by the gel can be compared to a pressure  $p_g$  in both the aggregate and the cracked zone (Fig. 5). As the pressure  $p_g$  is an isotropic stress, in the cracked zone filled by the gel

$$\sigma_{rr}^{cz}(R_{cz}) = \sigma_{\theta\theta}^{cz}(R_{cz}) \quad (22)$$

The imposed strains applied to the aggregate and to the cracked zone are the relative increase in the volume due to the production of gel by ASR. However, as explained above, a part of the gel fills the porous volume surrounding the aggregate (determined by Eq. (3)) and does not participate in the expansion. The imposed strain is then equal to the volume of gel  $V_g$  minus the connected porosity  $V_{por}$  filled by the gel compared to the volume of the aggregate. Thus, the last equation is given by chemical modeling:

$$\langle V_g - V_{por} \rangle^+ = \frac{4}{3}\pi R_a^3 \varepsilon_{imp1} + \frac{4}{3}\pi (R_{cz}^3 - R_a^3) \varepsilon_{imp2} \quad (23)$$

where  $\langle X \rangle^+$  is equal to  $X$  if  $X > 0$  or equal to 0 if  $X \leq 0$ .

The damage to the concrete is obtained by substituting the volume of gel determined by the chemical modeling (Eq. (3)) in Eq. (23). The expansion induced by ASR in each aggregate size fraction can thus be calculated. For the aggregate size fraction  $a$ :

$$\varepsilon_a = \frac{u_{rr}(R_{REV}^a)}{R_{REV}^a} \quad (24)$$

with  $R_{REV}^a$  the radius of the REV corresponding to the aggregate size fraction  $a$ .

If the concrete contains several aggregate size fractions, the resulting strain is assumed to be the sum of expansions induced by each fraction:

$$\varepsilon_{ASR} = \sum_a \varepsilon_a \quad (25)$$

The relationship between the damage and the expansion of one reactive aggregate obtained by this model has been plotted in Fig. 6. It

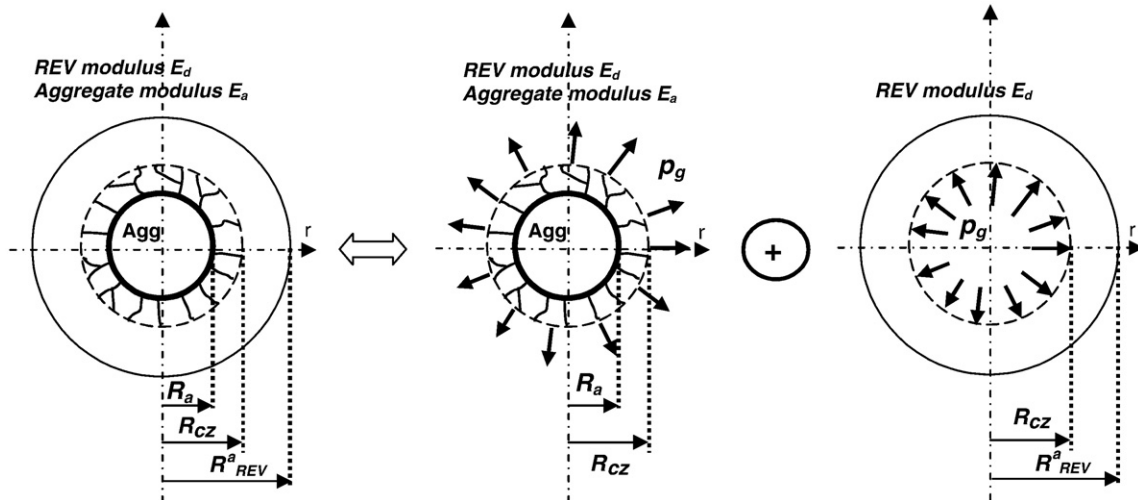


Fig. 5. Mechanical equilibrium of the damaged REV.

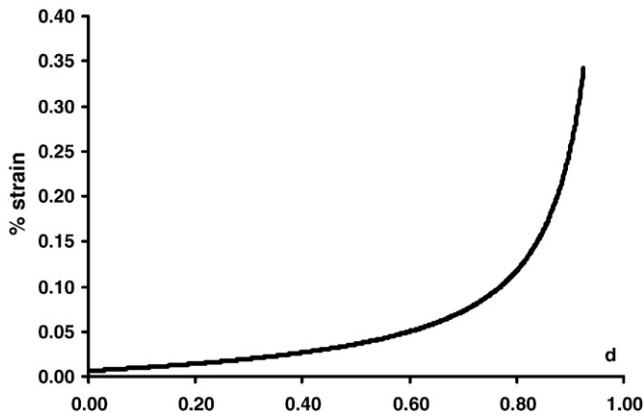


Fig. 6. Relationship between the damage ( $d$ ) and the expansion of the REV.

is interesting to compare these values to experimental data but only a few papers deal with the decrease of direct tensile strength with ASR expansion, and none with the decrease of the tensile modulus. Siemes and Visser measured a decrease greater than 85% in the direct tensile strength for expansions between 0.05% and 0.1% [37]. For the same ASR expansions (between 0.05 and 0.1%), the damage calculated by the model is between 60 and 75%, which is slightly lower than the experimental values.

The mechanical modeling uses only five parameters: the Young's modulus and the Poisson's coefficient of the aggregate and mortar ( $E_a$ ,  $\nu_a$  and  $E_m$ ,  $\nu_m$ ) and the tensile strength of the mortar  $f_t$ ; no other fitting is necessary.

## 5. Comparison with experiments

The last part of the paper shows some calculations performed with the model developed in the previous parts. In order to assess the capability of the model to represent and predict real ASR expansions, the analysis is divided into three parts. First, experiments used to fit and test the model are presented. Then, the identification of the parameters is carried out and discussed. For the identification, the measurements of expansion performed on four different mortars were used. Finally, the model is used to calculate the expansion of six other mortars. The calculated expansions are compared to the measured ones and the differences are discussed.

### 5.1. Experiments

The experiments used to check the capability of the model to predict ASR expansion have been presented and analyzed in a previous paper [38]. Therefore, only the parameters used by the model are dealt with here. Expansion was measured on mortar prisms with a water–cement ratio of 0.5. The sand and cement contents were 1613.4 kg/m<sup>3</sup> and 537.8 kg/m<sup>3</sup> respectively. Two distinct Na/Si ratios were studied by adjusting the alkali contents ( $\text{Na}_2\text{O}_{\text{eq}}$ ) to 6.2 and 13.4 kg of alkali per m<sup>3</sup> of mortar (addition of NaOH in the mixing water). Three size fractions of aggregate were used: FS for small aggregates (80–160  $\mu\text{m}$ ), FM for medium aggregates (315–630  $\mu\text{m}$ ) and FL for large ones (1.25–3.15 mm). The reactive aggregate was a siliceous limestone. In the experimental study, only fractions FS and FL were composed of reactive aggregates, the medium size aggregates were not reactive but were introduced into the formulation to obtain an acceptable particle size distribution. The reactive silica contents of the two reactive fractions were measured through a chemical analysis based on basic attack [38]; the reactive  $\text{SiO}_2$  contents were equal to 9.4% and 12.4%/kg of aggregate for FS and FL. The particle size distribution was the same for all the mortars: 30% of FS, 40% of FM and 30% of FL. Different proportions of reactive and non-reactive

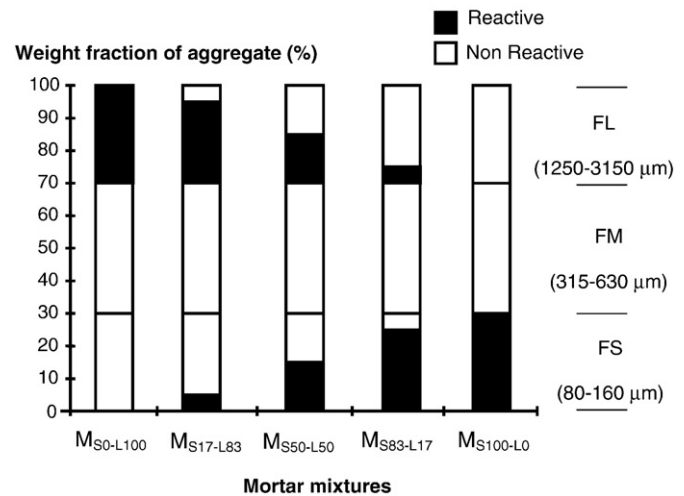


Fig. 7. Particle size distribution of the five mortars (in black: reactive aggregate, in white: non-reactive aggregate).

aggregates from the two size fractions FS and FL were used to make 5 reactive mortars for each alkali content, with always 30% of reactive particles (Fig. 7). The mortar  $M_{S0-L100}$  contained 0% of reactive particles in the SL fraction while 100% of the particles of the FL fraction were reactive. For the mortar  $M_{S100-L0}$ , 100% of the smallest reactive particles (FS) were reactive and all the other particles were non-reactive. The reactive particle contents of the mortars  $M_{S17-L83}$ ,  $M_{S50-L50}$  and  $M_{S83-L17}$ , lay between these two values. The ASR expansions presented in Figs. 8 and 9, and used for the identification

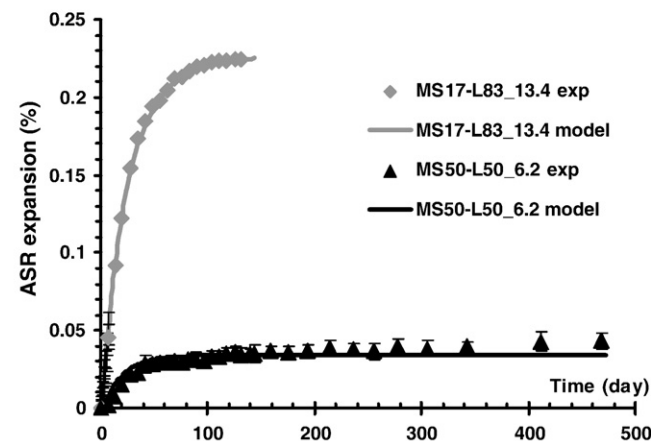
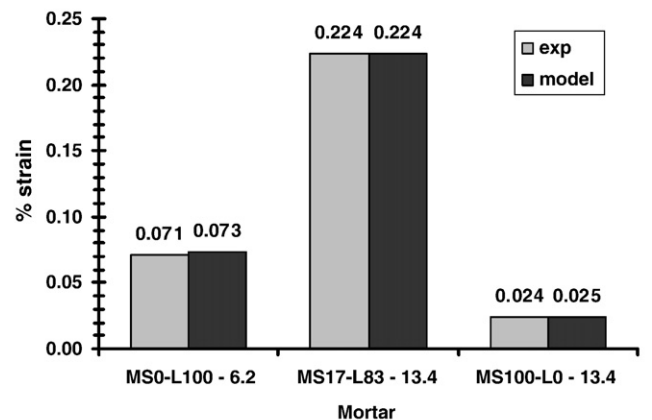


Fig. 8. Identification of chemical parameters on mortars  $M_{S0-L100} - 6.2 \text{ kg/m}^3$ ,  $M_{S50-L50} - 6.2 \text{ kg/m}^3$ ,  $M_{S17-L83} - 13.4 \text{ kg/m}^3$  and  $M_{S100-L0} - 13.4 \text{ kg/m}^3$ .

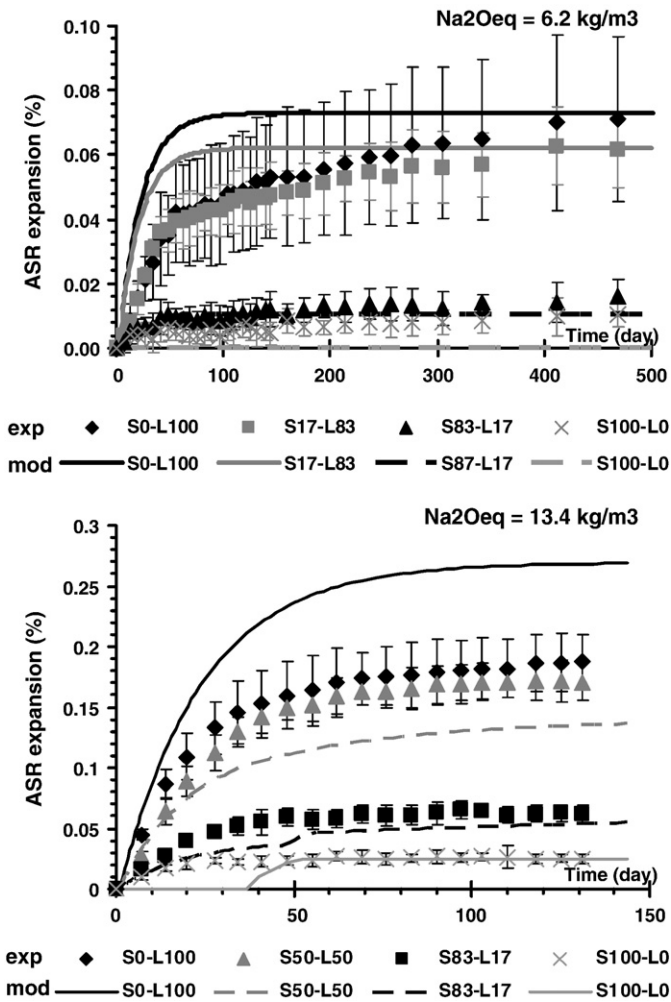


Fig. 9. Prediction of the ASR-expansion of the mortars  $M_{S0-L100}$ ,  $M_{S17-L83}$ ,  $M_{S83-L17}$ ,  $M_{S100-L0}$  – 6.2 kg/m<sup>3</sup> and  $M_{S0-L100}$ ,  $M_{S50-L50}$ ,  $M_{S83-L17}$ ,  $M_{S100-L0}$  – 13.4 kg/m<sup>3</sup>.

of the parameters and for the analysis of the model were obtained by subtracting the expansion of the reference mortar (without reactive aggregate) from the total expansion [38]. Thus, the strains were only caused by the pressure of the ASR gel and not by the pressure due to water absorption. The water porosity of each of the mortars was measured at the end of the experiment (Table 1), using AFPC–AFREM method [39]. Values were between 17 and 20%.

## 5.2. Assessment of the parameters

Table 2 sums up the various parameters of the two models, with the symbols, the method used for identification, the values and the units. The following parts explain how the values were obtained.

### 5.2.1. Parameters of the physicochemical modeling

The first parameters needed for the physicochemical modeling are given by the mix-design information (see above: size and volume

Table 1  
Porosity of the mortars in %.

Alkali content of the mix design	$M_{S0-L100}$	$M_{S17-L83}$	$M_{S50-L50}$	$M_{S83-L17}$	$M_{S100-L0}$
6.2 kg/m <sup>3</sup>	17.5	16.9	17.3	17.6	17.6
13.4 kg/m <sup>3</sup>	20	19.9	19.6	18.9	17.9

Table 2  
Parameter identification.

Parameter	Symbol	Identification	Value	Units
<b>Physicochemical modeling</b>				
<b>Aggregate</b>				
Coefficient of diffusion	$D$	Curve fitting	$3.5 \times 10^{-13}$	m <sup>2</sup> /s
Porosity	$p$	Usual value	0.01	%
<b>Paste</b>				
Porosity of mortar	$p_{mort}$	Measurement	17–20.	%
Thickness of the connected porous interface zone	$t_c$	Curve fitting	$0.63 \times 10^{-6}$	m
<b>Gel</b>				
Molar volume of ASR gel	$V_{gel}^{mol}$	Curve fitting	$18.2 \times 10^{-6}$	m <sup>3</sup> /mol
Alkali threshold	$Na_{th}$	Curve fitting	620.	mol/m <sup>3</sup>
Alkali fixation coefficient	$f$	Curve fitting	$-6.5 \times 10^{-7}$	m <sup>3</sup> /m <sup>3</sup> /s
<b>Mechanical modeling</b>				
<b>Aggregate</b>				
Young's modulus	$E_a$	Usual value	70,000.	MPa
Poisson's coefficient	$\nu_a$	Usual value	0.2	–
<b>Mortar</b>				
Young's modulus	$E_{REV}$	Usual value	9000.	MPa
Poisson's coefficient	$\nu_{REV}$	Usual value	0.2	–
Tensile strength	$f_t$	Usual value	3.	MPa

fractions of particles, alkali and reactive silica contents). Taking all the information into account, the aggregate concentration per m<sup>3</sup> of concrete  $C_{agg}$  could be calculated: it was equal to 0.61.

The porosity of the aggregate was taken as the value of 0.01% given by a previous work [40]. The porosity of the cement paste was calculated with Eq. (7). The last five parameters (coefficient of diffusion, thickness of the connected porous interface zone, molar volume of ASR gel, threshold concentration  $Na_{th}$  and alkali fixation coefficient) of the physicochemical modeling were obtained by curve fitting on four mortars of the experimental study as explained in Section 5.2.3.

### 5.2.2. Parameters of the mechanical modeling

All the parameters of the mechanical modeling (Table 2) were obtained from the literature. The Young's modulus of the siliceous limestone was determined in a previous experiment [41]. The instantaneous Young's modulus of the mortar was taken as equal to a frequently found value for a mortar with a ratio W/C of 0.5: about 27,000 MPa. As explained in the presentation of the assumptions, a long-term Young's modulus equal to one third of the instantaneous Young's modulus was used in the calculations in order to take the creep effect into account. The Poisson's coefficients of aggregate and mortar were taken as 0.2. The tensile strength of the mortar was estimated at 3 MPa. None of the parameters of the mechanical modeling were fitted.

### 5.2.3. Identification by curve fitting

The five parameters (coefficient of diffusion, thickness of the connected porous interface zone, molar volume of ASR gel, threshold concentration  $Na_{th}$  and alkali fixation coefficient) were obtained by curve fitting the expansions of four mortars of the experimental study: the last expansion measured on  $M_{S0-L100}$  with 6.2 kg/m<sup>3</sup> of alkali and  $M_{S100-L0}$  with 13.4 kg/m<sup>3</sup> of alkali, and the whole expansion curves of  $M_{S50-L50}$  with 6.2 kg/m<sup>3</sup> of alkali and  $M_{S17-L83}$  with 13.4 kg/m<sup>3</sup> of alkali (Fig. 8). First, the molar volume of ASR gel and the thickness of the connected porous zone were determined to fit the last expansion measured on the mortars  $M_{S0-L100}$  – 6.2 kg/m<sup>3</sup>,  $M_{S17-L83}$  and  $M_{S100-L0}$  – 13.4 kg/m<sup>3</sup> (Fig. 8). Then, the coefficients of diffusion and fixation of alkali were calculated to fit the whole kinetics of the expansion of the two mortars  $M_{S50-L50}$  – 6.2 kg/m<sup>3</sup> and  $M_{S17-L83}$  – 13.4 kg/m<sup>3</sup> (Fig. 8). The values thus determined are given in Table 2.



### 5.3. Discussion

#### 5.3.1. Curve fitting

As shown in Fig. 8, the determination of the five parameters of the physicochemical modeling allowed a good representation of ASR expansions to be obtained for two different reactive particle sizes and two different alkali contents. As already observed in the analysis of the experiment [38], the larger the aggregate, the higher the ASR-expansion. The model explains the decrease of the expansion with the increase in the reactive particle sizes by the movement of a part of the gel into the connected porous zone. The decrease of 90% observed between the small fraction FS and the large fraction FL can be obtained by a thickness of the connected porous zone of about 0.6  $\mu\text{m}$ . The second main parameter of the final expansions of the mortars in the model is the molar volume of ASR gels. The molar volume determined by curve fitting for this experiment,  $18.2 \cdot 10^{-6} \text{ m}^3/\text{mol}$ , is in good agreement with the experimental values obtained on synthetic gels. In [42], the molar volume of synthetic gels similar to natural ASR gels in solution was measured to be between  $17.35 \cdot 10^{-6}$  and  $23.65 \cdot 10^{-6} \text{ m}^3/\text{mol}$  depending on the composition of the gels. The two last parameters have large effects on the kinetics and on the expansion of mortar with low alkali content. Good representation of the expansion curves was obtained with the values given in Table 2.

The threshold of alkali above which the ASR-expansion occurred was assessed by curve fitting. With this threshold and all the parameters given in Table 2, for a mortar with a mean porosity of 18%, ASR expansion occurs for alkali content higher than 4 kg of alkali /  $\text{m}^3$  of concrete. This is in good agreement with the usual values given by the literature (3 and 5 kg /  $\text{m}^3$ ) [23–26].

#### 5.3.2. Prediction of other expansions

Once the curve fitting had been performed, all the other expansions were calculated without any additional fitting (Fig. 9). For the low alkali content, the kinetics appears to be overestimated but the final expansions are well predicted. For the high alkali content, the mortars  $M_{S50-L50}$  and  $M_{S83-L17}$  are quite well-estimated but the prediction of the mortar  $M_{S0-L100}$  is not good. The differences between the calculations and the measurements of the mortar  $M_{S50-L50}$  can be explained by the sensitivity of the model to the porosity of the cement paste. If the same porosity is taken for the mortar  $M_{S100-L0}$  used in the curve fitting and for the mortar  $M_{S50-L50}$ , the prediction is perfect for the two mortars. A variation of 1.5% of porosity (it is the difference between the two mortars of the high alkali content  $M_{S50-L50}$  and  $M_{S100-L0}$ ) gives a variation of about 0.03% in the calculated expansions. The scatter (the porosity of  $M_{S0-L100}$  lies between 19.5% and 20.7%) and the high value of porosity (about 20% for  $M_{S0-L100}$ ,  $M_{S17-L83}$  and  $M_{S50-L50}$  with the high alkali content) can be responsible for the difficulties experienced in obtaining better agreement for the two mortars  $M_{S0-L100}$  and  $M_{S50-L50}$ . The delay observed for the mortar  $M_{S100-L0}$  can be partly explained by the discretization of the particle sizes: in the present study only one average size was used for each aggregate size range (S, M or L). A better description of the size distribution of the finest particles could improve the modeling results.

#### 5.3.3. Interest and limitations of the model

The model presented here is mainly based on a previous model developed by Poyet et al. [18]. Several improvements can be noted. In this new model, some considerations have been modified:

- Due to the large difference in the diffusion coefficients of the aggregate and the cement paste, the concentration of alkali in the paste has been considered as homogeneous and is represented by a single variable (no more discretization of the paste around each aggregate like in [18]). The calculated values remain reliable, but the duration of calculation is largely reduced.

- In order to predict the difference of expansion, the mechanical part of the model presents in [18] was partly based on a parameter which depends on the size of the aggregates. Thus, it was not an intrinsic parameter of the material. In the new model, all the mechanical parameters are intrinsic, i.e. independent of the aggregate size. The expansions of aggregate of different size can be deduced without supplementary fitting.
- The definition of a threshold in alkali concentration allows the expansions of mortars containing different alkali contents to be calculated with a good accuracy. No previous models in the literature were tested on this point.

Contrary to the previous model [18], the improved new model presented in this paper allows the prediction of ASR expansions of mortars containing particles of different sizes.

However, the present model still has some limitations. One of the main difficulties in using the model presented above is the determination of the reactive silica content in the aggregate. A method was proposed in [38] for the siliceous limestone studied here, but improvements are still required, particularly to be used for other types of reactive aggregates.

Some papers have shown the replacement of the alkali by calcium in the ASR gels [8–10]. This phenomenon has little effect on the expansion obtained in the laboratory for short periods or for mortars with high alkali content because it appears to occur after long period of exposure. However, it can have important effects on the final expansion in real structures because, once free again, alkali can attack more reactive silica and new expansions are possible [6,7]. Therefore, it will be the next improvement made to the model.

Moreover, the model was developed with several assumptions (about the diffusion, the composition of the ASR gel, the mechanical properties of mortar under long-term loading, etc.). Supplementary investigations are needed before it can be applied to real structures. In particular, the effect of temperature on all the physicochemical and mechanical mechanisms needs to be analyzed (expansion measurements of mortars kept at several temperatures are currently in progress). This paper has shown the effect of the aggregate size on the prediction of the concrete expansion. It should be taken into account in the expert assessments of real structures already performed in [6,7]. Thus, it would be important to study the effects of the discretization of the aggregate size distribution on the expansion predicted.

### 6. Conclusion

This paper presents an improved empirical microscopic model of ASR expansions based on previous models. It proposes some improvements to take the fixation of alkali into account and to calculate the ASR expansion by means of a mechanical damage variable. The diffusion and the fixation of the alkali are assessed with the mass balance equation. A threshold alkali concentration, above which the formation of the gel starts, is defined; the speed of alkali fixation is assumed to be proportional to the difference between the alkali concentration in the aggregate and this threshold. The mechanical modeling uses a damage variable in order to determine the ASR expansion due to the volume of gel produced by the reaction and determined by the physicochemical part of the model. No parameter of the mechanical model needs fitting. Previous experimental research has been used to check the capability of the model. Four parameters of the physicochemical modeling were determined by curve fitting the expansion curves of four mortars of this experiment. These model parameters have a physical meaning and have been found to be close to previous measurements reported in the literature. The model can reproduce the decrease of expansion with the size of the aggregate, and the increase of expansion with the alkali content. The model is also able to predict the expansions of six other mortars containing two sizes of aggregate and cast with two alkali contents. These calculations have shown the sensitivity of the model to the mortar porosity. Finally, the

academic interest of the model lies in the fact that the significance of every assumed mechanism is explained and quantified.

Real structures containing large reactive aggregate (size about 100 mm) are currently being analyzed in the LMDC by using the same assumptions as in this model. In this approach, the largest aggregates are crushed and used to make new mortars with high alkali contents in order to quantify the reactive silica remaining in affected concrete aggregate as rapidly as possible [7]. Kinetics parameters are assessed on these mortars and the model is used to predict the expansion of larger aggregates with different alkali contents. Thus, the model could be used to predict the slow expansion of concrete in structures from the fast expansion of mortar observed in the laboratory.

## Notation

$a$	sub or superscript relative to the size fraction of the reactive aggregate
$C_{\text{agg}}$	volume fraction of all the aggregate per $\text{m}^3$ of concrete
$C_{\text{Na}}$	concentration of alkali
$C_{\text{Na}}^{\text{p}}$	alkali concentration in the cement paste
$CZ$	subscript relative to the cracked zone surrounding the reactive aggregate
$D$	coefficient of diffusion of alkalis into the aggregate
$d$	damaged variable
$\underline{\varepsilon}$	strain matrix for each material
$\varepsilon_a$	expansion induced by ASR in the aggregate $a$
$\varepsilon_{\text{ASR}}$	total expansion of the concrete
$\varepsilon_{\text{imp1}}$	imposed strain applied to the aggregate
$\varepsilon_{\text{imp2}}$	imposed strain applied to the cracked zone
$E$	Young's modulus
$E_d$	damaged Young's modulus
$\phi_a$	volume fraction of reactive aggregates with mean radius $R_a$
$f$	coefficient of fixation of alkali
$f_t$	tensile strength of the mortar
$\underline{I}$	unit matrix
$M_{\text{Na2O}}$	mass of equivalent alkali per $\text{m}^3$ of concrete
$M_{\text{Na2O}}^{\text{mol}}$	molar mass of equivalent alkali (equal to 0.062 kg/mol)
$\nu$	Poisson's coefficient of the medium
$N_a$	number of reactive aggregate $a$ in the final REV
$N_{a_{\text{th}}}$	alkali threshold above which the attack of reactive silica starts
$n_g^a$	number of moles of ASR-gel produced by the aggregate $a$
$p_{\text{agg}}$	porosity of the aggregate
$p_{\text{cp}}$	porosity of the cement paste
$p_{\text{mort}}$	porosity of the mortar
$R_a$	mean radius of the reactive aggregate of size fraction $a$
$R_{\text{REV}}$	REV radius corresponding to the aggregate size fraction $a$
$\underline{\sigma}$	stress matrix for each material
$S(C_{\text{Na}})$	depletion term which represents the alkali consumption
$SC$	subscript relative to the concrete surrounding the reactive aggregate
$S_r$	saturation degree
$t_c$	thickness of the connected porous volume filled by the gel
$u$	displacement
$V_g$	total volume of ASR gel produced
$V_{\text{gel}}^{\text{mol}}$	molar volume of the gel
$V_{\text{po}}$	volume of porosity filled by the gel
$\langle X \rangle^+$	equal to $X$ if $X > 0$ or equal to 0 if $X \leq 0$ .

## Acknowledgment

The authors are grateful to Electricité De France for supporting this work.

## References

- [1] P. Léger, P. Cote, R. Tinawi, Finite element analysis of concrete swelling due to alkali-aggregate reaction in dams, *Comput. Struct.* 60 (1996) 601–611.
- [2] S. Malla, M. Wieland, Analysis of an arch-gravity dam with a horizontal crack, *Comput. Struct.* 72 (1999) 267–278.
- [3] F. Ulm, O. Coussy, L. Kefei, C. Larive, Thermo-chemo-mechanics of ASR expansion in concrete structures, *ASCE J. Eng. Mech.* 126 (3) (2000) 233–242.
- [4] K. Li, O. Coussy, Concrete ASR degradation: from material modeling to structure assessment, *Concr. Sci. Eng.* 4 (2002) 35–46.
- [5] V. Saouma, L. Perotti, T. Shimp, Stress Analysis of concrete structures subjected to alkali-aggregate reactions, *ACI Struct. J.* 104 (5) (2007) 532–541.
- [6] E. Grimal, Caractérisation des effets du gonflement provoqué par la réaction alcali-silice sur le comportement mécanique d'une structure en béton, PhD thesis, Université Paul Sabatier Toulouse, France (2007).
- [7] A. Sellier, E. Bourdarot, S. Multon, M. Cyr, E. Grimal, Assessment of the residual expansion for expertise of structures affected by AAR, 13th Int. Conf AAR, Trondheim, Norway, 2008.
- [8] J. Duchesne, M.-A. Bérubé, Discussion of the Paper "The effectiveness of supplementary cementing materials in suppressing expansion due to ASR – part 1, concrete expansion and portlandite depletion", *Cem. Concr. Res.* 24 (8) (1994) 1572–1573.
- [9] B. Lagerblad, J. Trägardh, Slowly reacting aggregates in Sweden – mechanism and conditions for reactivity in concrete, 9th ICAAR, Concrete Society Publication CS 106, London, Great-Britain, 1992, pp. 570–578.
- [10] W.J. French, Maintenance of mobile alkali concentration in cement paste during alkali-aggregate reaction, Enclosure to Proc. 8th ICAAR, Kyoto, Japan, 1989.
- [11] P. Goltermann, Mechanical predictions on concrete deterioration. part 1: eigenstresses in concrete, *ACI Mater. J.* 91 (6) (1994) 543–550.
- [12] Z.P. Bazant, G. Zi, C. Meyer, Fracture mechanics of AAR in concretes with waste glass particles of different sizes, *ASCE J. Eng. Mech.* 126 (3) (2000) 226–232.
- [13] Y. Furusawa, H. Ohga, T. Uomoto, An analytical study concerning prediction of concrete expansion due to alkali-silica reaction, in: Malhotra (Ed.), 3rd Int. Conf. on Durability of Concrete, Nice, France, 1994, pp. 757–780, SP 145–40.
- [14] A. Nielsen, F. Gottfredsen, F. Thøgersen, Development of stresses in concrete structures with alkali-silica reactions, *Mater. Struct.* 26 (1993) 152–158.
- [15] A. Sellier, J.-P. Bournazel, A. Mébarki, Modelling the alkali aggregate reaction within a probabilistic frame-work, 10th ICAAR, Melbourne, Australia, 1996, pp. 694–701.
- [16] Z.P. Bazant, A. Steffens, Mathematical model for kinetics of alkali-silica reaction in concrete, *Cem. Concr. Res.* 30 (2000) 419–428.
- [17] A. Suwito, W. Jin, Y. Xi, C. Meyer, A mathematical model for the pessimum effect of ASR in concrete, *Concr. Sci. Eng.* 4 (2002) 23–34.
- [18] S. Poyet, A. Sellier, B. Capra, G. Foray, J.-M. Torrenti, H. Cognon, E. Bourdarot, Chemical modelling of alkali silica reaction: influence of the reactive aggregate size distribution, *Mater. Struct.* 40 (2007) 229–239.
- [19] L.S. Dent Glasser, N. Kataoka, The chemistry of alkali-aggregate reactions, 5th ICAAR, Cape Town, South Africa, 1981, p. S252/23.
- [20] S. Chatterji, 1979, The role of  $\text{Ca}(\text{OH})_2$  in the breakdown of portland cement concrete due to alkali-silica reaction, *Cem. Concr. Res.* 9 (1979) 185–188.
- [21] S. Diamond, ASR – Another look at mechanisms, 8th ICAAR, Kyoto, Japan, 1989, pp. 83–94.
- [22] T.N. Jones, A new interpretation of alkali-silica reaction and expansion mechanisms in concrete, *Chem. Ind.* 18 (1988) 40–44.
- [23] C.A. Rogers, R.D. Hooton, Reduction in mortar and concrete expansion with reactive aggregates due to alkali leaching, *Cem., Concr. Aggreg.* 13 (1) (1991) 42–49.
- [24] D.W. Hobbs, Deleterious alkali-silica reactivity in the laboratory and under field conditions, *Mag. Concr. Res.* 45 (163) (1993) 103–112.
- [25] M.D.A. Thomas, B.Q. Blackwell, P.J. Nixon, Estimating the alkali contribution from fly ash to expansion due to alkali-aggregate reaction in concrete, *Mag. Concr. Res.* 48 (177) (1996) 251–264.
- [26] M.H. Shehata, M.D.A. Thomas, The effect of fly ash composition on the expansion of concrete due to alkali-silica reaction, *Cem. Concr. Res.* 30 (7) (2000) 1063–1072.
- [27] S. Diamond, Alkali reactions in concrete – pore solution effects, 6th International Conference on AAR in Concrete, Copenhagen, Denmark, 1983, pp. 155–166.
- [28] P. Rivard, M.A. Bérubé, J.-P. Ollivier, G. Ballivy, Decrease of pore solution alkalinity in concrete tested for alkali-silica reaction, *Mater. Struct.* 40 (2007) 909–921.
- [29] S. Urhan, Alkali silica and pozzolanic reactions in concrete. Part 1 : interpretation of published results and an hypothesis concerning the mechanism, *Cem. Concr. Res.* 17 (1) (1987) 141–152.
- [30] N. Thaulow, U.-H. Jakobsen, B. Clark, Composition of alkali silica gel and ettringite in concrete railroad ties: SEM-EDX and X-ray diffraction analyses, *Cem. Concr. Res.* 26 (1996) 309–318.
- [31] H.F.W. Taylor, *Cement Chemistry*, Academic Press, London, 1990.
- [32] M. Kawamura, H. Fuwa, Effects of lithium salts on ASR gel composition and expansion of mortars, *Cem. Concr. Res.* 33 (2003) 919–919.
- [33] E. Grimal, A. Sellier, Y. Le Pape, E. Bourdarot, Creep shrinkage and anisotropic damage in AAR swelling mechanism, part I: a constitutive model, *ACI Mater. J.* 105 (3) (2008) 227–235.
- [34] BAEL "Règles techniques de conception et de calcul d'ouvrages et constructions en béton armé suivant la méthode des états limites", Fascicule 62 of CCTG, French design code, 1991, modified in 1999.
- [35] L.M. Kachanov, Introduction to continuum Damage Mechanics, Martinus Nijhoff Publishers, 1986.
- [36] J. Lemaître, J.-L. Chaboche, in: Dunod (Ed.), *Mécanique des Matériaux Solides*, 1988, Paris, France.

- [37] T. Siemes, J. Visser, Low tensile strength in older concrete structures with alkali-silica reaction, 11th ICAAR, Quebec, Canada, 2000, pp. 1029–1038.
- [38] S. Multon, M. Cyr, A. Sellier, N. Leklou, L. Petit, Coupled effects of aggregate size and alkali content on ASR expansion, *Cem. Concr. Res.* 38 (3) (2008) 350–359.
- [39] AFPC-AFREM (Association Française Pour la Construction — Association Française de Recherche et Essais sur les Matériaux de construction), Durabilité des bétons. Méthodes recommandées pour la mesure des grandeurs associées à la durabilité. Mesure de la masse volumique apparente et de la porosité accessible à l'eau. Compte-Rendu des Journées Techniques, Toulouse, 11–12 Décembre 1997, pp. 121–124.
- [40] S. Poyet, Etude de la dégradation des ouvrages en béton atteints de la réaction alcali-silice: approche expérimentale et modélisation numérique multi-échelle des dégradations dans un environnement hydrochemo-mécanique variable, PhD thesis, Université de Marne la Vallée, France (2003).
- [41] C. Larive, Apports combinés de l'expérimentation et de la modélisation à la compréhension de l'alcali-réaction et de ses effets mécaniques, Laboratoire Central des Ponts et Chaussées (Edt.), Ouvrage d'Art, Rapport OA 28, 1998.
- [42] A. Perruchot, P. Massard, J. Lombardi, Composition et volume molaire apparent des gels Ca-Si, une approche expérimentale, *C. R. Geoscience* 335 (2003) 951–958.